Disrupted cholinergic modulation can underlie abnormal gamma rhythms in schizophrenia and auditory hallucination

Lee, Jung Hoon

Allen Institute for Brain Science Seattle, WA, USA.

Jungl@alleninstitute.org

Abstract

Auditory hallucination, one of the common symptoms of schizophrenia, has been thought to be induced by the failure of corollary discharge. It is consistent with the 'dysconnectivity hypothesis' that disrupted interareal interactions among brain regions underlie schizophrenia symptoms. However, the exact mechanisms underlying corollary discharge and its relation to the pathophysiology of schizophrenia remain elusive. In this study we used a computational model of primary auditory cortex (A1) composed of pyramidal cells, fast-spiking (FS) and non-FS inhibitory interneurons to elucidate potential mechanisms by which disrupted corollary discharge generates auditory hallucination. Our simulation results suggest that disrupted cholinergic modulation accounts for abnormal gamma rhythms observed in people with schizophrenia. More importantly, in the model, top-down gamma rhythms suppress A1 responses in normal condition, but when cholinergic modulation is disrupted, they erroneously activate A1 instead of deactivating it. Based on our simulation results, we propose that disrupted cholinergic modulation can underline auditory hallucination.

Keywords: computational model; auditory hallucination; abnormal gamma rhythms in schizophrenia; cholinergic modulation; inhibitory cell types

1. Introduction

Positive symptoms of schizophrenia generate illusionary perception and distorted reality, and it has been believed that such illusions result from the erroneous activation of auditory system induced by the failure of corollary discharge/efferent copy (Ford & Mathalon, 2005). As the corollary discharge suppresses the responses of primary auditory cortex (A1) to self-generated speech or inner thoughts (Ford & Mathalon, 2005; Schneider, Nelson, & Moony, 2014), its failure leads to the inaccurate activation of A1 and other auditory system. This is consistent with the dysconnectivity hypothesis that disturbed interactions among brain areas underlie the pathophysiology of schizophrenia (Pettersson-Yeo, Allen, Benetti, McGuire, & Mechelli, 2011; P. J. Uhlhaas, 2013).

However, we still do not understand how disrupted corollary discharge causes auditory hallucination. Synchronous oscillatory activity in the gamma frequency band (alternatively known as gamma rhythms) has been proposed to subserve interareal communication (Fries, 2005), and top-down gamma rhythms from higher order cognitive areas to lower order sensory cortices were reported in vision (Gregoriou, Gottes, Zhou, & Desimone, 2008) and auditory (Roopun et al., 2010) systems. Together, these studies lead to the possibility that top-down gamma rhythms can mediate corollary discharge.

Indeed, gamma rhythms appear to be abnormal in schizophrenia patients (Pittman-Polletta, Kocsis, Vijayan, Whittington, & Kopell, 2015; P. Uhlhaas & Singer, 2010). For instance, the gamma band power in electroencephalography (EEG) induced by 40 Hz auditory click trains is lower in schizophrenia (Kwon et al., 1999; Vierling-Claassen, Siekmeier, Stufflebeam, & Kopell, 2008). In addition, Spencer (Spencer, 2011) found that the baseline gamma power in the pre-stimulus period is higher, not lower in schizophrenia, which is consistent with the enhanced connectivity in the

resting state networks (Andreou et al., 2015) and the higher absolute gamma synchrony (Flynn et al., 2008). Although the potential pathophysiology behind the reduction of stimulus-evoked gamma rhythms have been studied via computational models (Spencer, 2009; Vierling-Claassen et al., 2008), the underlying mechanisms of enhanced baseline gamma rhythms are poorly understood.

Top-down gamma rhythms can be the source of baseline gamma rhythms, as they are independent from sensory stimulus inputs. It suggests that enhanced baseline gamma rhythms result from the pathophysiology underlying distorted corollary discharge. To study this possibility, we used a model of superficial layers of A1 in which three cell types, pyramidal (Pyr) cells, FS and non-FS inhibitory interneurons, interact with one another. We first studied the potential mechanisms replicating the abnormal gamma rhythms in schizophrenia and then investigated their implications for the pathophysiology responsible for auditory hallucination.

2. Methods

We used the peer reviewed simulator named NEST (Gewaltig & Diesmann, 2007) to build a network model. All neuron models and synapse models are natively supported by NEST. As shown in Figure 1A, we implemented superficial layers of A1 and three external populations. Specifically, A1 consisting of 400 Pyr, 70 FS and 30 non-FS cells interacts with three external populations of 100 Pyr cells (ovals in Figure 1A). First, HC mimics the higher order cognitive areas and projects 45 Hz sinusoidal Poisson spike trains into A1, as unidirectional signals from an association cortex to A1 were found at ~45 Hz (Roopun et al., 2010). Second, SC mimics bottom-up thalamic inputs induced by 40 Hz auditory click trains and thus projects 40 Hz sinusoidal Poisson spike trains into A1. These sinusoidal Poisson spike trains are generated by NEST-native device named ‘sinusoidal Poisson generator’ with parameters in Table 1. Third, A1 Pyr cells project outputs to downstream

neurons. These synaptic connections approximate the cortico-cortical projection from A1 to higher order auditory/cognitive areas, as superficial layers project directly to the higher order areas (Felleman & Van Essen, 1991; Markov & Kennedy, 2013). For simplicity, we did not consider any recurrent connection in the three external populations.

2.1. Neuron models

All three inhibitory cell types are implemented by neuron models proposed by Hill and Tononi (Hill & Tononi, 2005). The 'HT' neuron is a point neuron with simplified Hodgkin–Huxley currents. For reference, we provide a brief review of the neuron model; see (Hill & Tononi, 2005) for details.

The neuronal dynamics obey Equation 1:

$$\frac{dV}{dt} = \frac{[-g_{Na}(V-E_{Na})-g_{KL}(V-E_K)-I_{syn}-I_{int}]}{\tau_m} - g_{spike}(V-E_k)/\tau_{spike}. \quad (1)$$

The membrane potentials (V), decayed exponentially with time scale τ_m, are regulated by sodium (Na) and potassium (K) leak currents with conductance (g_{Na} and g_{KL}) and reversal potentials (E_{Na} and E_K). The fast hyperpolarization current during spikes is simulated with a rectangular spike with a conductance (g_{spike}) and decaying time constant (t_{spike}). Synaptic events induce dual exponential responses (I_{syn}) in the target neurons which are described by rising (τ_1) and decaying time (τ_2) constants (Table 2). The reversal potentials for GABA and AMPA are -80 and 0 mV in the model. We did not consider NMDA synapses in the model. The intrinsic ion currents (Iint) are from the original model (Hill & Tononi, 2005).

Also, spike threshold (θ) evolves over time with equilibrium (θ_{eq}) and time constant (t_θ), as shown in Equation 2.

$$\frac{d\theta}{dt} = -(\theta - \theta_{eq})/\tau_{\theta} \quad (2)$$

The three cell types have different parameters listed in Table 3. We assume that cholinergic modulation innervates non-FS cells for experimental observations. First, basal forebrain, which provides cholinergic modulation to cortices (Sarter, Parikh, & Howe, 2009), mainly targets somatostatin positive (SST) interneurons (Chen, Sugihara, & Sur, 2015). Second, cholinergic modulation does not modulate the excitability of FS cells (Gulledge, Park, Kawaguchi, & Stuart, 2007). Third, acetylcholine innervates low-threshold spiking interneurons known to express SST via nicotinic receptors but does not modulate the excitability of FS cells (Xiang, Huguenard, & Prince, 1998).

2.2. Synaptic connections

All synapses in the model have static synaptic weights unlike the depressing synapses in the original model (Hill & Tononi, 2005). FS and non-FS cells provide fast and slowly decaying GABA connections on target neurons, respectively (Traub et al., 2005); 7 msec and 20 msec are chosen for decay time constants for fast and slow kinetics (Table 2). According to the observed pattern (Pfeffer, Xue, He, Huang, & Scanziani, 2013), non-FS cells corresponding to SST cells inhibit FS and Pyr cells, whereas FS cells inhibit FS cells and Pyr cells. These two inhibitory cell types are also consistent with the two functional groups (major regulator and inhibitory selective interneurons) from a recent survey (Jiang et al., 2015). Figure 1A shows the schematic of synaptic connections. When we connect pre-synaptic and post-synaptic populations, we connect cell pairs randomly using connection probabilities (Table 4).

2.3. Simulation of local field potentials

We approximated EEG by calculating local field potentials (LFPs). LFPs were simulated by summing up all the synaptic currents in downstream neurons (Mazzoni, Panzeri, Logothetis, & Brunel, 2008). Then the spectral power density of LFPs was calculated via 'scipy' included in python. For each simulation condition, we ran 100 simulations, in which a network is independently instantiated using the same connectivity rule, and reported the average LFP power from them.

2.4. Spike-triggered average of LFPs

The coherence between top-down gamma rhythms to A1 and synaptic inputs to downstream neurons was measured with spike-triggered average (STA) of LFPs. In each simulation, we aggregated the 100 msec LFP segments aligned to the spike times of HC cell population which projects top-down gamma rhythms into A1 and averaged them to calculate STA of LFPs. The spectral power of STA of LFPs is calculated in each simulation, and we report the averaged power from 100 independent simulations.

3. Results

The goal of this study is to infer the pathophysiology responsible for auditory hallucination from abnormal gamma rhythms in schizophrenia. It has been inspired by 1) our earlier computational model study suggesting that disrupted cholinergic modulation accounts for the reduction of gamma rhythms in response to 40 Hz auditory click trains and 2) the hypothetical links between cholinergic modulation and the pathophysiology of schizophrenia (Martin & Freedman, 2007). Here we study the possibility that the disrupted cholinergic modulation can also underlie the enhanced baseline gamma rhythms (Spencer, 2011) by utilizing a network model shown in Figure 1A. As seen in the figure, SST cells inhibit FS and Pyr cells, whereas FS cells inhibit FS cells and

Pyr cells via cell type specific connectivity (Pfeffer et al., 2013). The three cell types, implemented with HT neurons (Hill & Tononi, 2005), exhibit disparate responses to 20 pA tonic currents (Figure 1B); see Methods for details on neuron models. The most active cells are FS cells, and non-FS cells show frequency adaptation, which is consistent with experimental observation (Gibson, Beierlein, & Connors, 1999; Kawaguchi & Kubota, 1997).

We simulate top-down and bottom-up gamma rhythms using sinusoidal Poisson spike trains independently (Methods). In the model, HC and SC cell populations are implemented to generate and project those sinusoidal Poisson spike trains onto A1. HC cells generate 45 Hz gamma rhythms mimicking top-down signals from an association cortex to A1 (Roopun et al., 2010). SC cells project 40 Hz gamma rhythms mimicking synaptic inputs into A1 induced by auditory click trains, as in an earlier experimental study (Kwon et al., 1999; Spencer, 2011). That is, top-down and bottom-up gamma rhythms are 45 and 40 Hz, respectively. According to experimental data (Couey et al., 2007; Gulledge et al., 2007; Xiang et al., 1998), we assumed that cholinergic modulation depolarizes non-FS cells and reduced the excitability to simulate the disrupted cholinergic modulation in A1. Specifically, non-FS cells receive 100 Hz Poisson spike trains in the control condition, whereas those external inputs are removed in the pathological conditions (Table 3).

Using this model, we ask if disrupted cholinergic modulation could account for the enhanced baseline gamma rhythms as well as the reduced stimulus-evoked gamma rhythms and study the implications of disrupted cholinergic modulation for auditory hallucination.

3.1. The reduced excitability of non-FS cells modulates gamma rhythms generated by A1 in the pre-stimulus and stimulus periods

In the first set of simulations, HC cells project top-down 45 Hz gamma rhythms onto A1 during the entire duration (1 second), whereas SC cells project bottom-up gamma rhythms for the last 500 msec. That is, the first 500 msec is the pre-stimulus period, and the last 500 msec is the stimulus period. The pre-stimulus period simulation results are used to calculate the baseline gamma rhythms, while the stimulus period simulation results are used to calculate the stimulus-evoked gamma rhythms. Figure 2A and B show the spikes of three cell types during simulations in the control and pathological conditions, respectively. Non-FS cells fire asynchronously in the control condition (Figure 2A), but they are quiescent in the pathological condition. FS cell activity appears to be stronger in the pathological condition, which can be explained by the difference in inhibition from non-FS cells to FS cells between the two conditions. Pyr cell activity also seems stronger in the pathological condition.

To examine the strength of gamma power induced in the downstream neurons, we estimated LFPs (in the downstream neurons) in the pre-stimulus and stimulus periods, respectively. As synaptic currents onto Pyr cells are the dominant factor for both LFPs and EEG (Destexhe & Bedard, 2013), we approximate EEG using LFPs calculated from the network model (Methods); we report the mean value of the power spectra from 100 independent simulations. In the pre-stimulus period, 45 Hz rhythms are induced by top-down gamma rhythms, and these induced rhythms are bigger in the pathological condition than in the control condition (Figure 2C), which is consistent with the enhanced baseline gamma rhythms (Spencer, 2011). We note that Pyr cells fire more strongly but more asynchronously in the pre-stimulus period when non-FS cells are active, accounting for the weaker baseline gamma-band power in the control condition (Figure 2C). In the stimulus period, 45 Hz rhythms are reduced, and 40 Hz rhythms, consistent with bottom-up gamma rhythms, are generated (Figure 2D). That is, A1 responds to bottom-up gamma rhythms rather than top-down

gamma rhythms in the stimulus period. More importantly, as seen in Figure 2D, 40 Hz rhythms induced by the bottom-up gamma rhythms are higher in the control condition, consistent with reduced stimulus-evoked gamma rhythms (Kwon et al., 1999; Vierling-Claassen et al., 2008).

3.2. What roles do non-FS cells play in modulating A1 outputs?

The results above suggest that the reduced non-FS cells' excitability accounts for abnormal gamma rhythms in schizophrenia. Then, what functions do non-FS cells perform in sensory signal processing? To better understand their functional roles, we ran simulations with varying inhibition strengths from non-FS cells to FS cells and from non-FS cells to Pyr cells. Figure 3 shows the spectral power of LFPs depending on the strengths of inhibition of non-FS cells. First, LFP power in the pre-stimulus period decreases, as non-FS-Pyr cell connections strengthen (Figure 3A). That is, non-FS cells prevent Pyr cells from responding to top-down gamma rhythms by directly inhibiting Pyr cells. Second, the strength of inhibition onto FS cells is positively correlated with LFP power in the stimulus period (Figure 3B), indicating that inhibition from non-FS cells to FS cells enhances the sensitivity of A1 Pyr cells to bottom-up gamma rhythms. As bottom-up inputs are introduced in the stimulus period only, we propose that non-FS cells ensure Pyr cells to fire strongly only when the bottom-up signals are presented.

3.3. Top-down gamma rhythms can subserve corollary discharge

To gain insight on potential functions of top-down gamma rhythms in the pre-stimulus period, we estimated the effects of top-down gamma rhythms on Pyr cells' spontaneous activity. In this experiment condition, Pyr cells are driven purely by external background inputs (Table 3), and the top-down gamma rhythms are projected onto A1 between 200-1000 msec during 2200 msec-long simulations. Figure 4A shows an example from our simulation results. During the top-down

gamma rhythm projection (200-1000 msec), FS cell activity is enhanced, but Pyr cell activity is reduced, indicating that top-down gamma rhythms suppress Pyr cell activity by innervating FS cells; this is consistent with the experimental observation that corollary discharge suppresses A1 activity by stimulating FS cells (Schneider et al., 2014). To test this assertion further, we consider the effects of top-down gamma rhythms as a function of the amplitudes of top-down gamma rhythms (Methods). Figure 4B shows how effectively top-down gamma rhythms suppress Pyr cell activity. *R* in the y-axis is the average firing rate of Pyr cells between 200-1000 msec divided by those between 1200-2000 msec when no top-down gamma rhythms are projected. The mean values of *R* from 100 simulations decrease, as the amplitude of top-down gamma rhythms generated by HC cells increases, confirming that gamma rhythms are suppressive of Pyr cell activity. That is, top-down gamma rhythms can subserve corollary discharge.

Lastly, does the disrupted cholinergic modulation disturb corollary discharge mediated by top-down gamma rhythms? The simulation results in Figure 3A suggest that non-FS cells prevent Pyr cells from responding to top-down gamma rhythms. Thus, we hypothesize that Pyr cells in A1 respond to top-down gamma rhythms when cholinergic modulation is disrupted in A1. To address this hypothesis, we estimated the spike-triggered average (STA) of LFPs (see Methods) using HC cells' spikes. This STA measures how reliably top-down gamma rhythms entrain A1 Pyr cells. The peak spectral power of STA of LFPs is at 45 Hz (Figure 4C), indicating that top-down gamma rhythms impinging onto A1 sometimes entrain A1 Pyr cells and thus induce synaptic inputs in the downstream neurons. More importantly, this power of STA of LFPs reflects the level of erroneous activation of A1 in response to top-down gamma rhythms and is enhanced (Figure 4C).

4. Discussion

This current model confirms that disrupted cholinergic modulation can underlie the reduction of stimulus-evoked gamma rhythms in schizophrenia, which was proposed by our earlier model study (Lee, Whittington, & Kopell, 2015), and further suggests that the same pathophysiology can account for the enhanced baseline gamma rhythms in schizophrenia (Spencer, 2011). Our results are also consistent with the hypothetical links between nicotine and the pathophysiology of schizophrenia (Martin & Freedman, 2007). Since acetylcholine can depolarize non-FS cells via nicotinic receptors (Couey et al., 2007; Xiang et al., 1998), the hypofunction of nicotinic receptors reduces the excitability of non-FS cells and thus induces abnormal A1 responses, as discussed above. This may also account for the procognitive effects of smoking, which increases the excitability of non-FS cells vis nicotinic receptors, in patients with schizophrenia (Sacco, Bannon, & George, 2004).

Below we discuss the implications of our simulation results for positive and negative symptoms of schizophrenia.

4.1. Implications for positive symptoms

A1 responses are suppressed by corollary discharge (Nelson et al., 2013; Schneider et al., 2014) and thus would be abnormally strong when the corollary discharge is disturbed. In the model, disrupted cholinergic modulation leads to the stronger erroneous activation of A1 in response to top-down gamma rhythms (Figure 4C). This result supports the hypothetical link between corollary discharge and auditory hallucination (Blakemore, Smith, Steel, Johnstone, & Frith, 2000; Ford & Mathalon, 2005) and further suggests that auditory hallucination reflects the content of top-down signals. More specifically, if top-down signals subserving corollary discharge mediate inner speech (Cho & Wu, 2013), A1 could turn this imaginary information into real sensory signals in the pathological condition; A1 is indeed hyperactive during hallucination (Ait Bentaleb,

Beauregard, Liddle, & Stip, 2002; Dierks et al., 1999). This explains the potential mechanisms by which the aberrant corollary discharge induces auditory hallucination in human voice. This notion is further supported by the observation that abnormal baseline gamma rhythms have been found stronger in the left-hemisphere (Spencer, 2011), which is associated with language processing.

4.2. Implications for negative symptoms

A1 responses to sensory stimuli are reduced in the pathological condition, impacting auditory perception directly. Could it be related to negative symptoms of schizophrenia? A precise correlation between A1 responses and negative symptoms of schizophrenia may prove difficult to find, but the reduction of A1 responses could impair some developmental processes. If the primary sensory responses are weaker than the normal ones, the developing mechanisms relying on the external stimuli could be impaired. In this way, the reduced A1 responses may contribute to schizophrenia's negative symptoms.

4.3. The limits of the model and future direction

It should be noted that we ignore the potential contribution of N-methyl-D-aspartate (NMDA) receptor hypofunction despite the well-known observation that the pathology of schizophrenia involves NMDA receptor hypofunction (Jadi, Margarita Behrens, & Sejnowski, 2015; Pittman-Polletta et al., 2015). This exclusion is due to the lack of information on the functional roles of NMDA synapses and their complex modulation of gamma rhythms (Hunt & Kasicki, 2013; Kirli, Ermentrout, & Cho, 2014). As NMDA antagonist modulate gamma rhythms in orbitofrontal and anterior cingulate cortices (Wood, Kim, & Moghaddam, 2012), we plan to extend our model to incorporate these cognitive areas and investigate the coordination between NMDA receptors and

cholinergic gating in the auditory perception, with which we could explore more implications for schizophrenia's 'dysconnections' among brain regions.

Acknowledgments

We wish to thank the Allen Institute founders, Paul G. Allen and Jody Allen, for their vision, encouragement and support.

References

Ait Bentaleb, L., Beauregard, M., Liddle, P., & Stip, E. (2002). Cerebral activity associated with auditory verbal hallucinations: A functional magnetic resonance imaging case study. *Journal of Psychiatry and Neuroscience*, *27*(2), 110–115.

Andreou, C., Nolte, G., Leicht, G., Polomac, N., Hanganu-Opatz, I. L., Lambert, M., … Mulert, C. (2015). Increased Resting-State Gamma-Band Connectivity in First-Episode Schizophrenia. *Schizophrenia Bulletin*, *41*(4), 930–939. http://doi.org/10.1093/schbul/sbu121

Blakemore, S. J., Smith, J., Steel, R., Johnstone, C. E., & Frith, C. D. (2000). The perception of self-produced sensory stimuli in patients with auditory hallucinations and passivity experiences: evidence for a breakdown in self-monitoring. *Psychological Medicine*, *30*(5), 1131–9. http://doi.org/10.1017/S0033291799002676

Chen, N., Sugihara, H., & Sur, M. (2015). An acetylcholine-activated microcircuit drives temporal dynamics of cortical activity. *Nature Neuroscience*, *18*(6), 892–902. http://doi.org/10.1038/nn.4002

Cho, R., & Wu, W. (2013). Mechanisms of auditory verbal hallucination in schizophrenia.

Frontiers in Psychiatry, *4*(NOV), 1–8. http://doi.org/10.3389/fpsyt.2013.00155

Couey, J. J., Meredith, R. M., Spijker, S., Poorthuis, R. B., Smit, A. B., Brussaard, A. B., & Mansvelder, H. D. (2007). Distributed Network Actions by Nicotine Increase the Threshold for Spike-Timing-Dependent Plasticity in Prefrontal Cortex. *Neuron*, *54*(1), 73–87. http://doi.org/10.1016/j.neuron.2007.03.006

Damaraju, E., Allen, E. A., Belger, A., Ford, J. M., McEwen, S., Mathalon, D. H., … Calhoun, V. D. (2014). Dynamic functional connectivity analysis reveals transient states of dysconnectivity in schizophrenia. *NeuroImage: Clinical*, *5*(July), 298–308. http://doi.org/10.1016/j.nicl.2014.07.003

Destexhe, A., & Bedard, C. (2013). Local field potential. *Scholarpedia*, *8*(8), 10183.

Dierks, T., Linden, D. E., Jandl, M., Formisano, E., Goebel, R., Lanfermann, H., & Singer, W. (1999). Activation of Heschl's gyrus during auditory hallucinations. *Neuron*, *22*(3), 615–621. http://doi.org/10.1016/S0896-6273(00)80715-1

Felleman, D. J., & Van Essen, D. C. (1991). Distributed hierarchical processing in the primate cerebral cortex. *Cerebral Cortex (New York, N.Y. : 1991)*, *1*(1), 1–47. Retrieved from http://www.ncbi.nlm.nih.gov/pubmed/1822724

Flynn, G., Alexander, D., Harris, A., Whitford, T., Wong, W., Galletly, C., … Williams, L. M. (2008). Increased absolute magnitude of gamma synchrony in first-episode psychosis. *Schizophrenia Research*, *105*(1-3), 262–71. http://doi.org/10.1016/j.schres.2008.05.029

Ford, J. M., & Mathalon, D. H. (2005). Corollary discharge dysfunction in schizophrenia: Can it explain auditory hallucinations? *International Journal of Psychophysiology*, *58*(2-3 SPEC.

ISS.), 179–189. http://doi.org/10.1016/j.ijpsycho.2005.01.014

Fries, P. (2005). A mechanism for cognitive dynamics: neuronal communication through neuronal coherence. *Trends in Cognitive Sciences*, *9*(10), 474–80. http://doi.org/10.1016/j.tics.2005.08.011

Gewaltig, M.-O., & Diesmann, M. (2007). NEST (NEural Simulation Tool). *Scholarpedia*, *2*(4), 1430.

Gibson, J. R., Beierlein, M., & Connors, B. W. (1999). Two networks of electrically coupled inhibitory neurons in neocortex. *Nature*, *402*(6757), 75–9. http://doi.org/10.1038/47035

Goñi, J., van den Heuvel, M. P., Avena-Koenigsberger, A., Velez de Mendizabal, N., Betzel, R. F., Griffa, A., … Sporns, O. (2014). Resting-brain functional connectivity predicted by analytic measures of network communication. *Proceedings of the National Academy of Sciences of the United States of America*, *111*(2), 833–8. http://doi.org/10.1073/pnas.1315529111

Gregoriou, G. G., Gottes, S. J., Zhou, H., & Desimone, R. (2008). visual cortex during attention. *Science*, *324*(5931), 1207–1210. http://doi.org/10.1126/science.1171402.

Gulledge, A. T., Park, S. B., Kawaguchi, Y., & Stuart, G. J. (2007). Heterogeneity of Phasic Cholinergic Signaling in Neocortical Neurons, 2215–2229. http://doi.org/10.1152/jn.00493.2006.

Hill, S., & Tononi, G. (2005). Modeling Sleep and Wakefulness in the Thalamocortical System. *Journal of Neurophysiology*, *93*(3), 1671–1698. http://doi.org/10.1152/jn.00915.2004

Hunt, M. J., & Kasicki, S. (2013). A systematic review of the effects of NMDA receptor

antagonists on oscillatory activity recorded in vivo. *Journal of Psychopharmacology (Oxford, England)*, *27*(11), 972–86. http://doi.org/10.1177/0269881113495117

Jadi, M. P., Margarita Behrens, M., & Sejnowski, T. J. (2015). Abnormal Gamma Oscillations in N-Methyl-D-Aspartate Receptor Hypofunction Models of Schizophrenia. *Biological Psychiatry*, *79*(9), 716–726. http://doi.org/10.1016/j.biopsych.2015.07.005

Jiang, X., Shen, S., Cadwelll, C., Berence, P., Sinz, F., Ecker, A. S., … Tolias, A. S. (2015). Principles of connectivity among morphologically defined cell types in adult neocortex. *Science*, *350*(6264).

Kawaguchi, Y., & Kubota, Y. (1997). GABAergic cell subtypes and their synaptic connections in rat frontal cortex. *Cerebral Cortex (New York, N.Y. : 1991)*, *7*(6), 476–86. Retrieved from http://www.ncbi.nlm.nih.gov/pubmed/9276173

Kirli, K. K., Ermentrout, G. B., & Cho, R. Y. (2014). Computational study of NMDA conductance and cortical oscillations in schizophrenia. *Frontiers in Computational Neuroscience*, *8*(October), 133. http://doi.org/10.3389/fncom.2014.00133

Kwon, J. S., O'Donnell, B. F., Wallenstein, G. V., Greene, R. W., Hirayasu, Y., Nestor, P. G., … McCarley, R. W. (1999). Gamma Frequency–Range Abnormalities to Auditory Stimulation in Schizophrenia. *Archives of General Psychiatry*, *56*(11), 1001. http://doi.org/10.1001/archpsyc.56.11.1001

Lee, J. H., Whittington, M. A., & Kopell, N. J. (2015). Potential Mechanisms Underlying Intercortical Signal Regulation via Cholinergic Neuromodulators. *Journal of Neuroscience*, *35*(45), 15000–15014. http://doi.org/10.1523/JNEUROSCI.0629-15.2015

Markov, N. T., & Kennedy, H. (2013). The importance of being hierarchical. *Current Opinion in Neurobiology*, *23*(2), 187–94. http://doi.org/10.1016/j.conb.2012.12.008

Martin, L. F., & Freedman, R. (2007). Schizophrenia and the alpha7 nicotinic acetylcholine receptor. *International Review of Neurobiology*, *78*(06), 225–46. http://doi.org/10.1016/S0074-7742(06)78008-4

Mazzoni, A., Panzeri, S., Logothetis, N. K., & Brunel, N. (2008). Encoding of naturalistic stimuli by local field potential spectra in networks of excitatory and inhibitory neurons. *PLoS Computational Biology*, *4*(12), e1000239. http://doi.org/10.1371/journal.pcbi.1000239

Nelson, A., Schneider, D. M., Takatoh, J., Sakurai, K., Wang, F., & Mooney, R. (2013). A circuit for motor cortical modulation of auditory cortical activity. *The Journal of Neuroscience : The Official Journal of the Society for Neuroscience*, *33*(36), 14342–53. http://doi.org/10.1523/JNEUROSCI.2275-13.2013

Pettersson-Yeo, W., Allen, P., Benetti, S., McGuire, P., & Mechelli, A. (2011). Dysconnectivity in schizophrenia: Where are we now? *Neuroscience and Biobehavioral Reviews*, *35*(5), 1110–1124. http://doi.org/10.1016/j.neubiorev.2010.11.004

Pfeffer, C. K., Xue, M., He, M., Huang, Z. J., & Scanziani, M. (2013). Inhibition of inhibition in visual cortex: the logic of connections between molecularly distinct interneurons. *Nature Neuroscience*, *16*(8), 1068–76. http://doi.org/10.1038/nn.3446

Pittman-Polletta, B. R., Kocsis, B., Vijayan, S., Whittington, M. A., & Kopell, N. J. (2015). Brain rhythms connect impaired inhibition to altered cognition in schizophrenia. *Biological Psychiatry*, *77*(12), 1020–1030. http://doi.org/10.1016/j.biopsych.2015.02.005

Roopun, A. K., Lebeau, F. E. N., Ramell, J., Cunningham, M. O., Traub, R. D., & Whittington, M. a. (2010). Cholinergic neuromodulation controls directed temporal communication in neocortex in vitro. *Frontiers in Neural Circuits*, *4*(March), 8. http://doi.org/10.3389/fncir.2010.00008

Sacco, K. A., Bannon, K. L., & George, T. P. (2004). Nicotinc receptor mechanisms and cognition in normal states and neuropsychiatric disorders. *J Psychopharmacol.*, *18*(4), 457–474.

Sarter, M., Parikh, V., & Howe, W. M. (2009). Phasic acetylcholine release and the volume transmission hypothesis: time to move on. *Nature Reviews. Neuroscience*, *10*(5), 383–90. http://doi.org/10.1038/nrn2635

Schneider, D., Nelson, A., & Moony, R. (2014). A synaptic and circuit basis for corollary discharge in the auditory cortex. *Nature*, *513*, 189–194.

Spencer, K. M. (2009). The functional consequences of cortical circuit abnormalities on gamma oscillations in schizophrenia: insights from computational modeling. *Frontiers in Human Neuroscience*, *3*(October), 33. http://doi.org/10.3389/neuro.09.033.2009

Spencer, K. M. (2011). Baseline gamma power during auditory steady-state stimulation in schizophrenia. *Frontiers in Human Neuroscience*, *5*(January), 190. http://doi.org/10.3389/fnhum.2011.00190

Traub, R. D., Contreras, D., Cunningham, M. O., Murray, H., LeBeau, F. E. N., Roopun, A., … Whittington, M. a. (2005). Single-column thalamocortical network model exhibiting gamma oscillations, sleep spindles, and epileptogenic bursts. *Journal of Neurophysiology*, *93*(4),

2194–232. http://doi.org/10.1152/jn.00983.2004

Uhlhaas, P. J. (2013). Dysconnectivity, large-scale networks and neuronal dynamics in schizophrenia. *Current Opinion in Neurobiology*, *23*(2), 283–290. http://doi.org/10.1016/j.conb.2012.11.004

Uhlhaas, P., & Singer, W. (2010). Abnormal neural oscillations and synchrony in schizophrenia. *Nature Reviews Neuroscience*, *11*, 100–113.

van den Heuvel, M. P., & Hulshoff Pol, H. E. (2010). Exploring the brain network: A review on resting-state fMRI functional connectivity. *European Neuropsychopharmacology*, *20*(8), 519–534. http://doi.org/10.1016/j.euroneuro.2010.03.008

Vierling-Claassen, D., Siekmeier, P., Stufflebeam, S., & Kopell, N. (2008). Modeling GABA alterations in schizophrenia: a link between impaired inhibition and altered gamma and beta range auditory entrainment. *Journal of Neurophysiology*, *99*, 2656–2671. http://doi.org/10.1152/jn.00870.2007

Wood, J., Kim, Y., & Moghaddam, B. (2012). Disruption of Prefrontal Cortex Large Scale Neuronal Activity by Different Classes of Psychotomimetic Drugs. *The Journal of Neuroscience*, *32*(9), 3022–3031. http://doi.org/10.1523/JNEUROSCI.6377-11.2012

Xiang, Z., Huguenard, J. R., & Prince, D. A. (1998). Cholinergic Switching Within Neocortical Inhibitory Networks. *Science*, *281*(5379), 985–988. http://doi.org/10.1126/science.281.5379.985

Legends

Figure 1: The structure of the model. (A) The superficial layer of A1 is explicitly modeled using three cell types (Pyr, FS and non-FS cells in red, blue and green, respectively). In the model, there are three external populations (shown as ovals) of Pyr cells interacting with A1. The first two populations (HC and SC) project top-down and bottom-up gamma rhythms into A1, and each individual Pyr cell in the populations fires inhomogeneous Possion spikes rate of either 40 Hz or 45 Hz depending on the population. The last population (downstream neurons) receives synaptic inputs from A1 Pyr cells. (B) The firing patterns of the three cell types in response to 20 pA tonic current injection.

Figure 2: The network responses depending on the excitability of non-FS cells. (A) The red, blue and green dots represent action potentials of Pyr, non-FS and FS cells in the control condition. Each row in the y-axis is the ids of cells. (B) Action potentials in the pathological condition. (C) The comparison of the spectral power of LFPs in the pre-stimulus period between the control and pathological conditions; the scale of LFP power is arbitrary. (D) The comparison of LFP power between the two conditions. The averaged power spectra from 100 simulations is displayed.

Figure 3: The effects of inhibition of non-FS cells. (A) The modulation LFP power via inhibition from non-FS to FS cells in the pre-stimulus period. (B) The modulation of LFP power via inhibition from non-FS to Pyr cells in the stimulus period. The averaged power spectra from 100 simulations is displayed.

Figure 4: The functional roles of top-down gamma rhythms. (A) Spike activity with top-down gamma rhythms introduced between 200-1000 msec indicated by the black arrow. (B) The reduction of Pyr cell activity depending on amplitudes of top-down gamma rhythms. (C) The spectral power of STA of LFP using spikes of top-down gamma rhythms.

Table 1: Parameters for sinusoidal Poisson generator. This NEST-native device (Gewaltig & Diesmann, 2007) generates inhomogeneous oscillatory spike trains depending on the three parameters, 'amplitude (ac)', 'baseline (dc)' and 'frequency'. For HC and SC, we use the values shown below.

Table 2: Synaptic parameters. All synapses are static and induce double exponential responses described by τ_1 and τ_2. g_{peak} and E_{rev} are the conductance of the synapses and reversal potentials.

Table 3: Neuronal parameters. We list the parameters chosen for the three cell types. g_T is the conductance of low-threshold currents (Hill & Tononi, 2005), and the frequency of external background inputs to each cell type is shown in the last column. All cells are implemented using NEST-native neuron models named "ht_neurons" (Gewaltig & Diesmann, 2007), and non-specified parameters are the same as defaults values in NEST.

Table 4: Connectivity. Connections are randomly generated using the following connectivity. The weights are used to scale synaptic strength (Gewaltig & Diesmann, 2007).

Tables

Table 1

	Amplitude (Hz)	Baseline (Hz)	Frequency (Hz)
HC	60	0	45
SC	60	0	40

Table 2

	g_{peak}	τ_1	τ_2	E_{rev} (mV)
AMPA	0.1	0.5	2.4	0
GABA from FS	0.33	1.0	7.0	-80
GABA from non-FS	0.33	1.0	20.0	-80

Table 3

	NaP	t_{spike}	θ_{eq} (mV)	τ_m (msec)	τ_θ (msec)	g_T	Ext (Hz)
Pyr	1.0	2.0	-51	16.0	2.0	2.0	200
FS	1.0	2.0	-53	8.0	1.0	1.0	100
Non-FS	1.0	2.0	-53	8.0	1.0	2.0	100

Table 4

Connection type	Connection probability	Weights
External background	N/A	3.0
Pyr→Pyr	0.4	0.075
Pyr→FS	0.4	0.45
Pyr→non-FS	0.2	0.15
FS→FS	1.0	0.15
FS→Pyr	0.4	0.6
Non-FS→FS	0.4	0.6
Non-FS→Pyr	0.4	0.39
HC to Pyr	0.2	0.09
HC to FS	0.2	0.18
SC to Pyr	0.2	0.18
SC to FS	0.2	0.18
Pyr→downstream	0.2	0.15

Figures

Figure 1

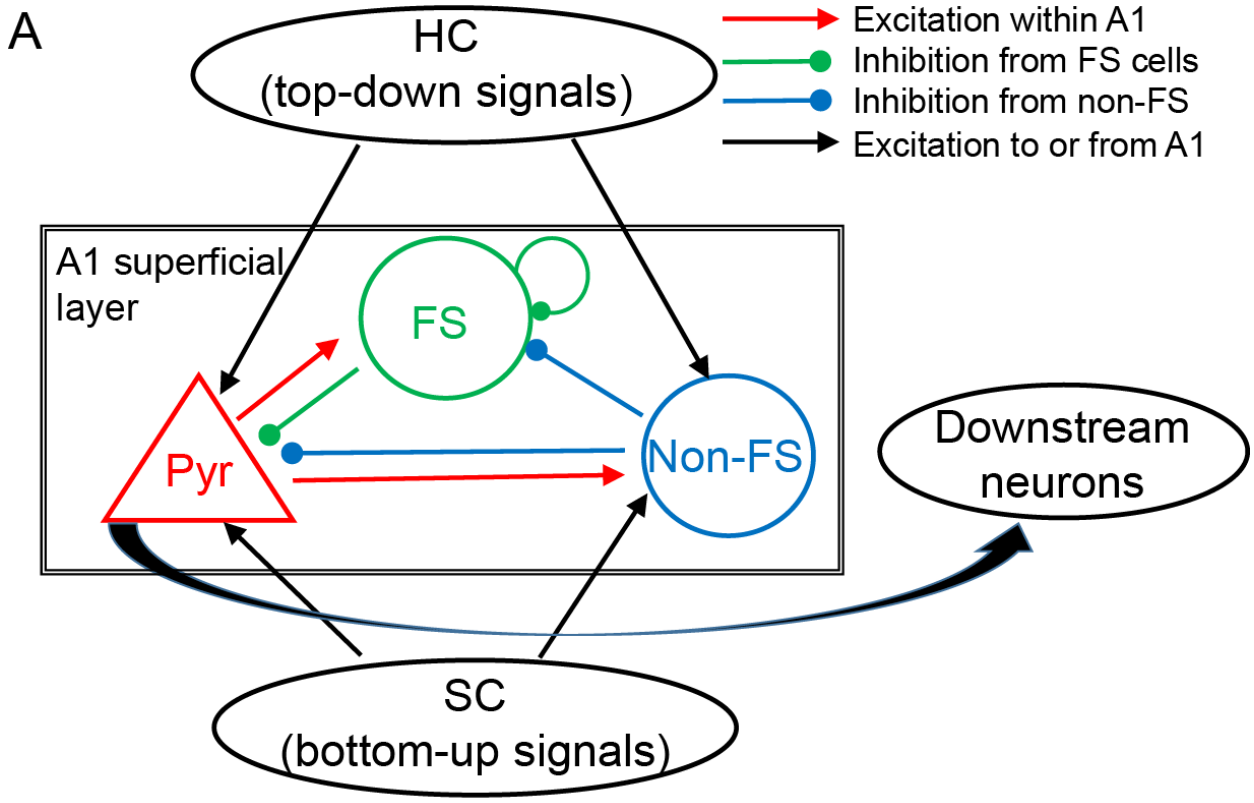

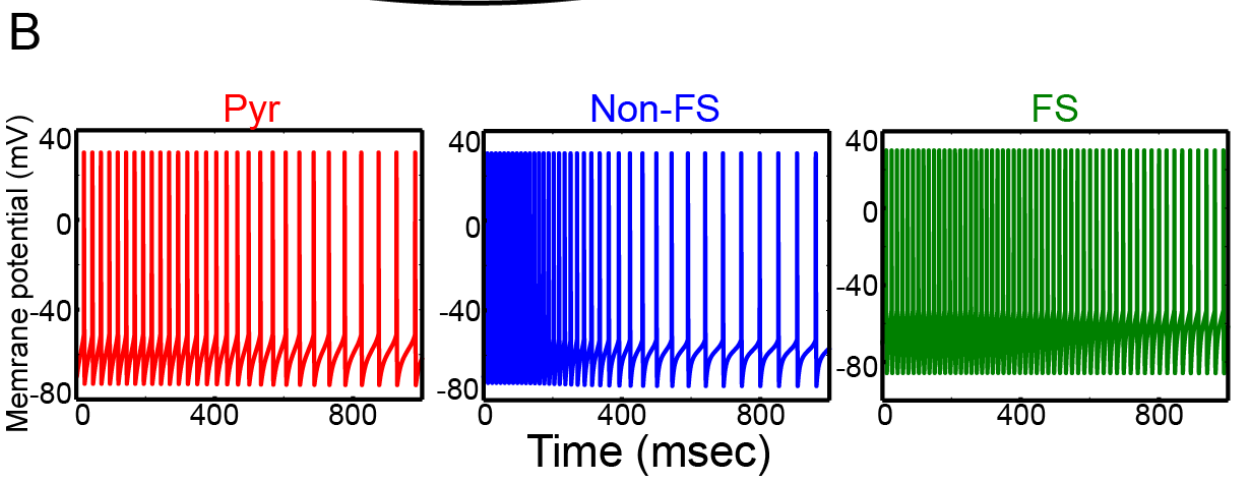

Figure 2

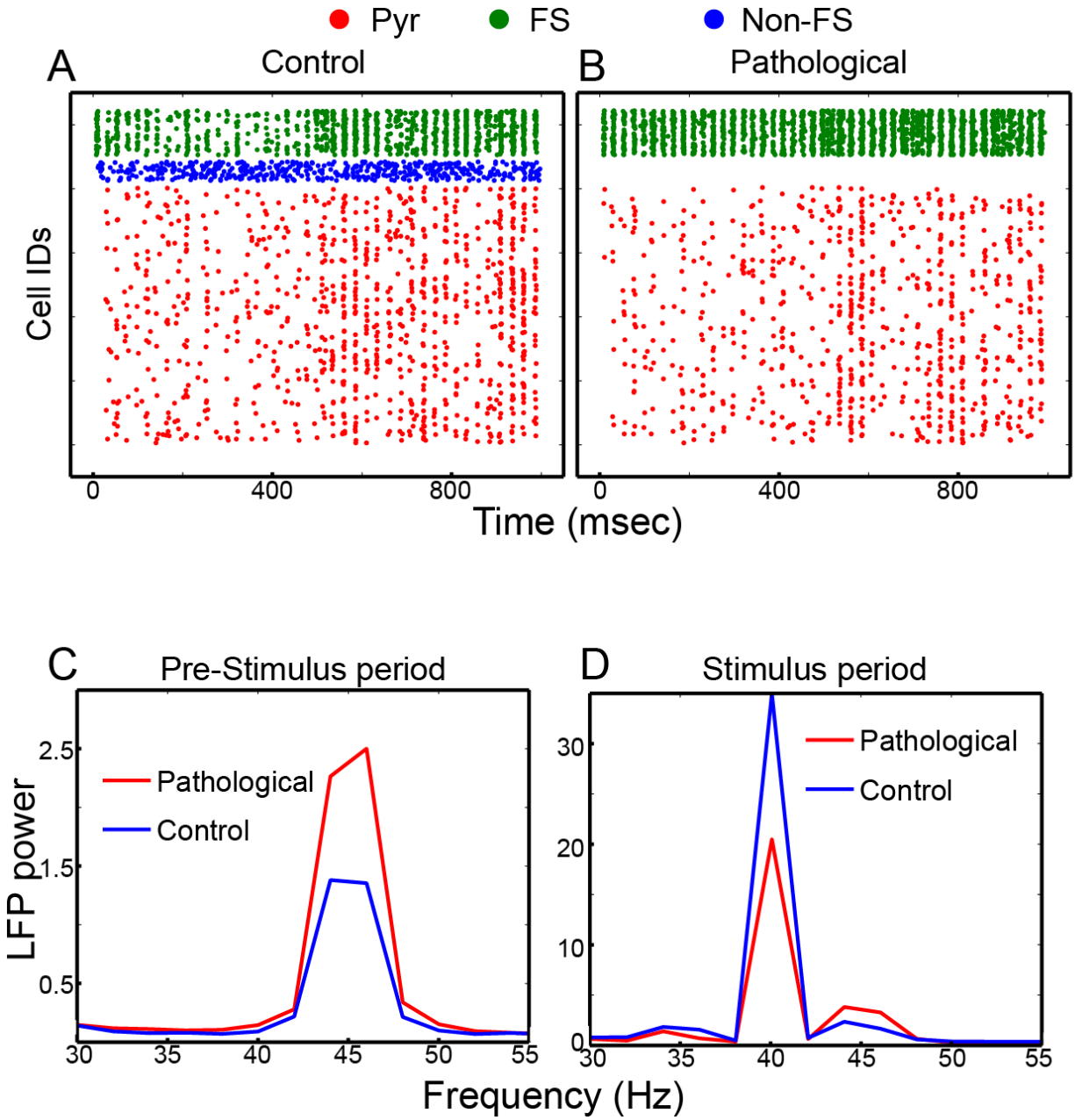

Figure 3

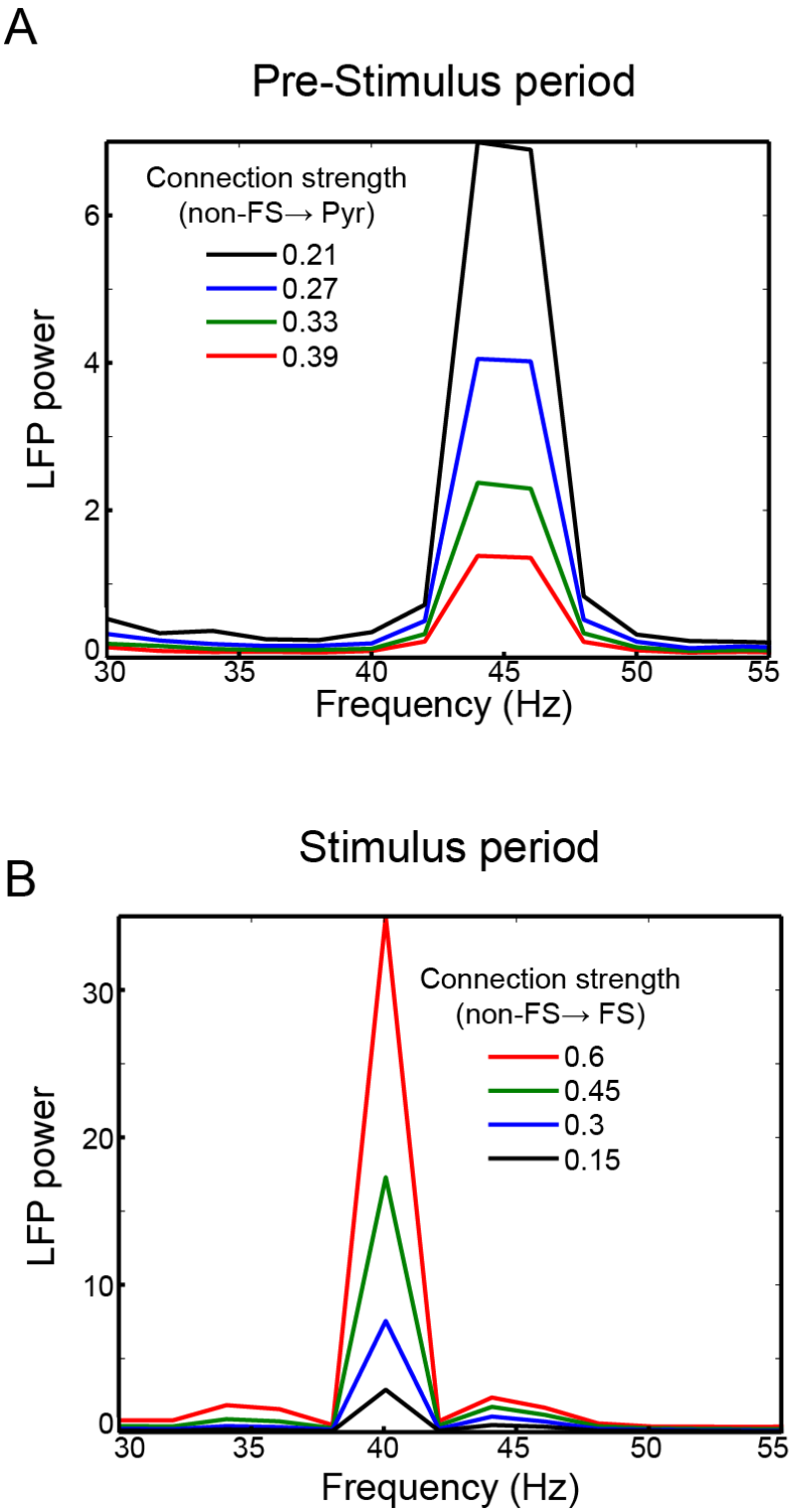

Figure 4